Portable cyber-physical system for indoor and outdoor gas sensing

Topias Järvinen[a], Gabriela Simone Lorite[a], Anne-Riikka Rautio[a], Koppány Levente Juhász[b,c], Ákos Kukovecz[b,d], Zoltán Kónya[b,c], Krisztian Kordas[a], Geza Toth[a,*]

[a]Microelectronics Research Unit, P.O. Box 4500, 90014 University of Oulu, Finland

[b]Department of Applied and Environmental Chemistry, MTA-SZTE "Lendület" Porous Nanocomposites Research Group, University of Szeged, Hungary

[c]MTA-SZTE Reaction Kinetics and Surface Chemistry Research Group, University of Szeged, Hungary

[d]MTA-SZTE "Lendület" Porous Nanocomposites Research Group, University of Szeged, Hungary

[*]Corresponding author: geza.toth@oulu.fi

Abstract

A design, development and testing process for a cyber-physical system capable of versatile gas sensor measurement is described. Two approaches for the system are proposed; a stationary system for calibration and testing in laboratory environments and a portable system with wireless capability. The device utilizes a well-established Arduino microcontroller as well as a Raspberry Pi single board computer. The functionality is realized with C and Python programming languages. The operability is validated by system performance evaluation in the mixture of air and hydrogen gas, using both commercial and experimental Taguchi-type metal oxide semiconductor sensors. The experimental sensors are fabricated by inkjet printing platinum decorated tungsten oxide nanoparticles onto an electrode pattern on a silicon substrate which is then wire bonded to a chip carrier. The measurement platform demonstrated in our paper provides rapid prototyping capabilities for evaluating novel gas sensor materials in realistic measurement scenarios.

Keywords: cyber-physical systems, gas sensors, embedded systems.

1. Introduction

Gas sensing is a key process in safety and environmental monitoring systems [1–5]. Metal oxide semiconductor materials have been utilized in gas sensor applications since the first results with zinc oxide (ZnO) and tin oxide (SnO_2) powders in the 1950s [6–9]. Since then material scientists have been extensively investigating novel materials and methods in order to enhance the sensitivity and selectivity of gas sensors. Both properties are equally important for safety and reliability in several applications. For instance, combustion processes in furnaces and vehicle engines are adjusted by monitoring the composition of exhaust gases. To be able to efficiently research, prototype and verify

the performance of novel materials in these actual scenarios, a user-friendly and affordable platform would be a great help for engineers and scientists working in the field.

Cyber-physical systems (CPS) integrate embedded systems and physical processes. Over the years, engineering researchers have pioneered the development of miniaturized and powerful embedded systems while computer scientists have reported innovative approaches in networking and software development. CPS research faces the challenge to integrate these fields into highly reliable and efficient systems towards applications such as critical infrastructural, traffic, and safety control, process automation as well as advanced automotive/aerospace systems [10–13]. The functionality of a CPS transverses from physical occurrence at the sensor input, data processing and feedback to the intercommunication between the modules and transmitting the results outwards to the user.

There are various monitoring and controlling systems utilizing gas sensors which can be considered cyber-physical systems such as environmental monitoring, combustion process controlling and indoor air quality monitoring. These systems might consist of a single sensor device or a network of individual sensor nodes. The scope of designing these systems is very broad, spanning from the materials research of the sensor chips to the control electronics and computer engineering related to the Internet of Things (IoT) nature of the operations. It is challenging to include the whole design chain in a research topic.

In this work, we designed, manufactured and validated an operational CPS for gas sensor measurements, capable of both indoors and outdoors measurements without the need of complex laboratory equipment. The implementation utilizes well established microcontroller platforms and custom electronics design for accompanying sensors with diverse requirements. Two innovative approaches have been implemented: (i) a stationary device for sensor calibration and, (ii) a device acting as independent and wireless battery-powered measurement system. Both systems were designed to couple with a separate circuit board which houses the sensors. The implemented systems were validated using commercial and custom-made experimental Taguchi -type sensors.

2. Design and manufacturing of the CPS

The hardware structure design for the stationary system as well as the fully wireless system is shown in Figure 1. The stationary CPS (YÚN platform) was designed to be used in indoors environment and, therefore, was plugged into the mains. On the other hand, the fully wireless system (Raspberry pi platform) was designed to be used as an independent, portable and fully wireless device for both indoors and outdoors applications. Printed circuit boards (PCB) were designed for each system to act as an interface between the platform and sensor board. The microcontroller unit (MCU) for each platform was selected by considering the available community support and the level of integration (e.g. on-board Wi-Fi chip). The sensor board was designed to comply with either of the systems. Both systems were designed to record the measurement data to a microSD card as well as upload it to cloud via Wi-Fi. The custom printed circuit boards were designed with KiCad (Version 3.0.2).

The modular design of the presented CPS allows easy assembly of all the components to one device. The boards were stacked and connected via standard pinouts. The sensor board could also be attached

to the interface boards via serial cable, allowing calibration in a test chamber with a serial feedthrough. In addition, both systems were equipped with thin-film transistor (TFT) displays for visualizing the data. Finally, 3D printed cases were designed with Autodesk Inventor Professional 2016 (Autodesk 2016) and printed from acrylonitrile butadiene styrene (ABS) filament by using a Makerbot Replicator X2 (MakerBot Industries).

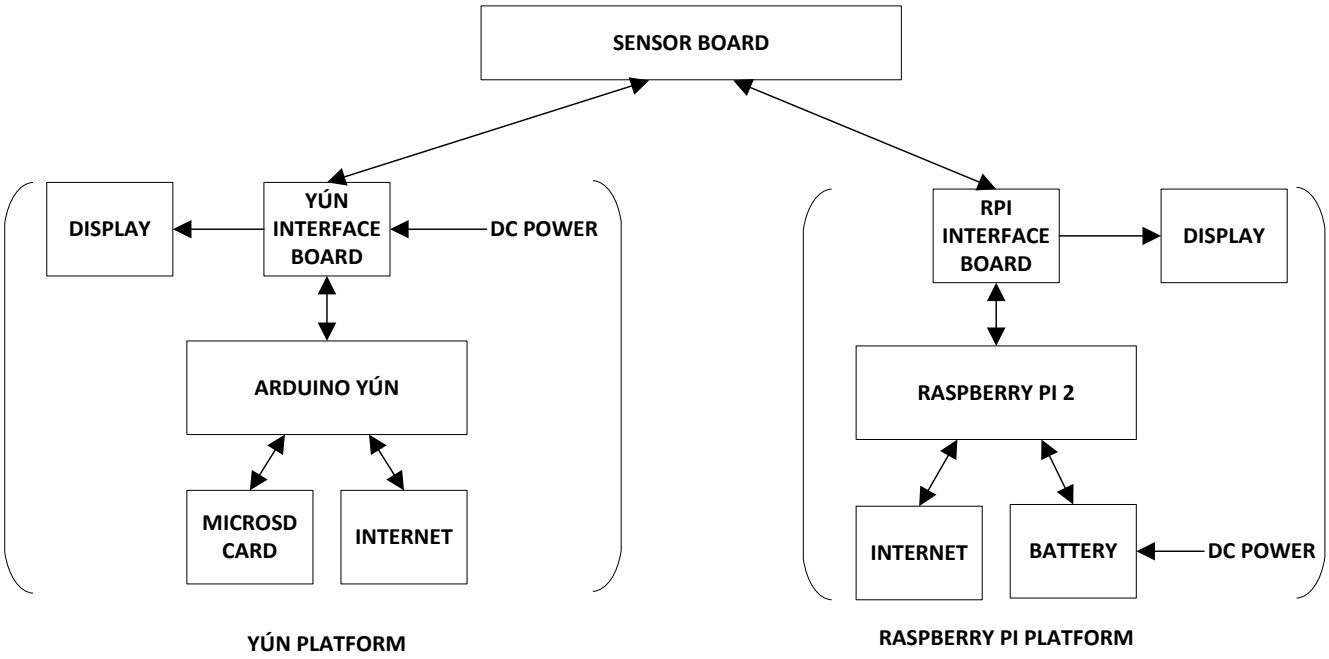

Figure 1 Scheme for representing the system hierarchies of Yún and Raspberry Pi platforms. Both systems are compatible with a common sensor board.

2.1 Stationary system

The stationary CPS was implemented by using Arduino Yún platform (Arduino LLC) which is based on Atmel ATmega32u4 microcontroller. In addition, this platform includes Atheros AR9331 processor, which runs an embedded Linux distribution.

This system incorporates an interface board similar to so-called shields. Those are often used in microcontroller applications, providing easy access to various peripherals while coupling the standard pinout of the microcontroller to enable further stacking of circuit boards. This pinout pattern was utilized in the design of the interface board. The main function of the interface board is to provide the connectivity between the microcontroller and the sensor board. Additionally the platform includes a power regulator for input voltages up to 15 V which is converted to the operating voltages of 5 and 3.3 V. The schematic diagram and the completed system is shown in Figure 2.

The microcontroller is programmed with C in Arduino integrated development environment (IDE). The software controls the PWM duty cycles for heating circuits and polls the measurement data from the analog-to-digital converter (ADC). Data is saved on a microSD card and shown on a display. On

the side of embedded Linux a script written with Python communicates with a Dropbox application (Dropbox Inc.). The script periodically uploads the data file to the cloud service.

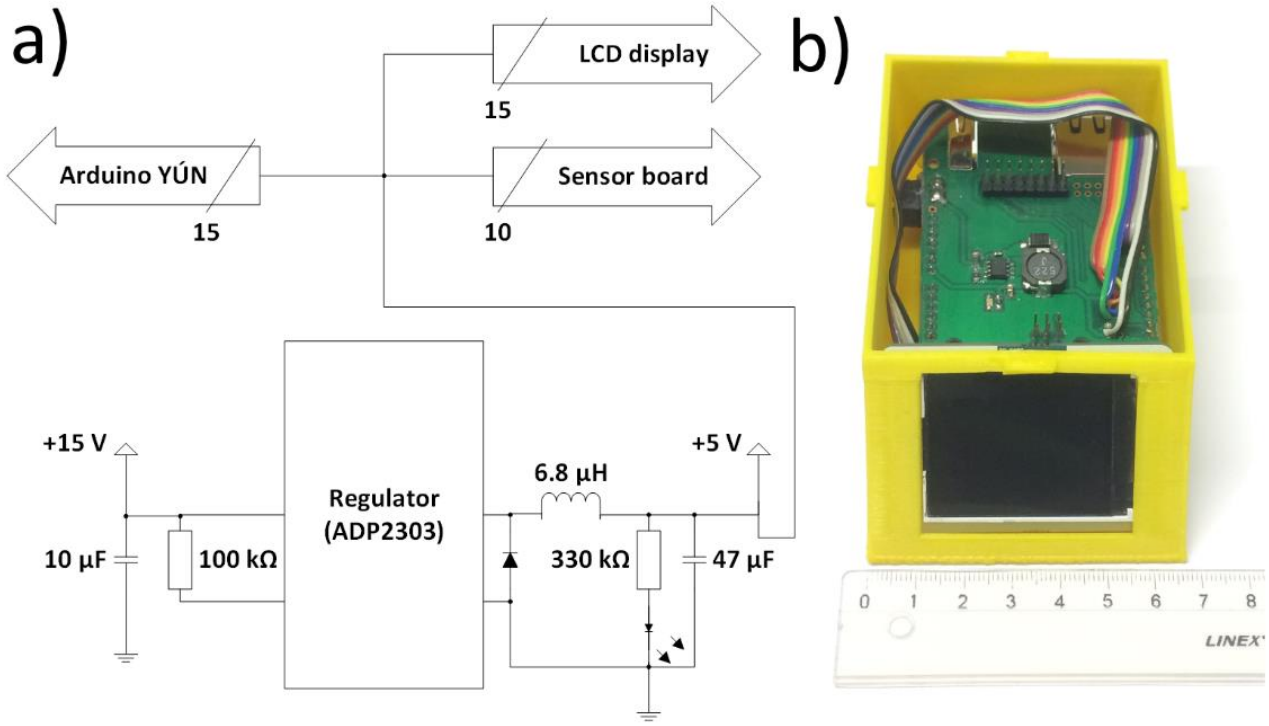

Figure 2 (a) The schematic diagram of the Yún interface board and (b) the completed stationary system assembly without the sensor board.

2.2 Fully wireless system

The fully wireless system was implemented by using Raspberry Pi 2 platform (Raspberry Pi Foundation). In this system, an Atmel ATMEGA328P-PU MCU was placed on the interface board in order to standardize the interaction to the sensor board. The measurement data is forwarded to the Raspberry Pi platform via serial connection. This platform also includes a quad-core ARM processor running an embedded Linux distribution. In addition, wireless functionality is provided by a Wi-Fi adapter connected to an USB port.

The wireless system utilizes a similar interface board as described in 2.1. In this case the interface board complies with the Raspberry Pi layout. The included microcontroller handles the communication between the Raspberry Pi and the components on the sensor board, performing the similar functions as the microcontroller on stationary system. Instead of a power regulator, a battery pack with integrated loading electronics is fitted under the circuit boards and it supplies the operating voltage of 5 V via the interface board. The final weight of the system with sensor board attached was 415 g. The schematic of the interface board is shown in Figure 3(a) and the complete system assembly in Fig. 3(b).

On the Raspberry Pi platform there is a Python program which displays the measurement data as graphs on the display. This user interface utilizes the PyQtGraph library [14]. The same program uploads the data file to the cloud service.

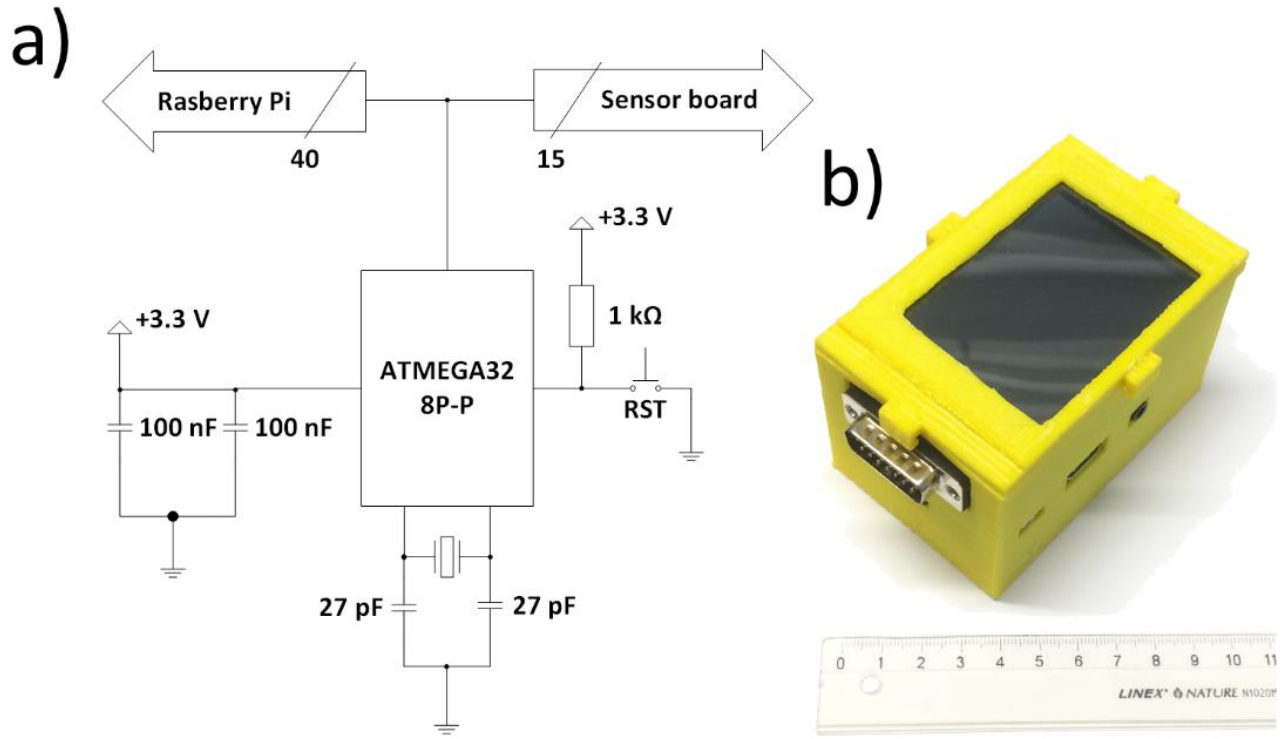

Figure 3 (a) The schematics diagram of the Raspberry Pi interface board and (b) the complete encased system assembly without sensor board.

2.3 Sensor board

The sensor board design included four socketed sensors enabling to evaluate distinct gases simultaneously. Since temperature and humidity can affect the gas sensor resistance curves, a combined temperature and humidity sensor (DHT22, Aosong Electronics Co., Ltd) was added to the sensor board in order to calibrate the measurements according to the environmental conditions. The load resistances for gas sensors were implemented with trimmer potentiometers for adjusting the sensitivity range of the sensors. In order to simplify the sensor box interface and allow for precise conversion, a discrete 10-bit ADC (MCP3008, Microchip Technology Inc.) was included. The ADC does not require any external components. However, to achieve reliable high impedance measurement with the ADC, a 100 nF capacitor was added parallel to each load resistance, which somewhat slows down the refresh data rate allowing for 10 ms measuring intervals or longer.

Usually commercial gas sensors have a heating resistor coil operating in the 1-5 V range depending on the sensor. In order to support a wide range of sensors, a pulse width modulation (PWM) outputs from microcontrollers were utilized to provide different voltage levels. The PWM outputs were amplified with a metal-oxide semiconductor field effect transistors (MOSFET) since the microcontroller cannot provide sufficient current on the output. The schematics diagram and completed PCB assembly is depicted in Figure 4.

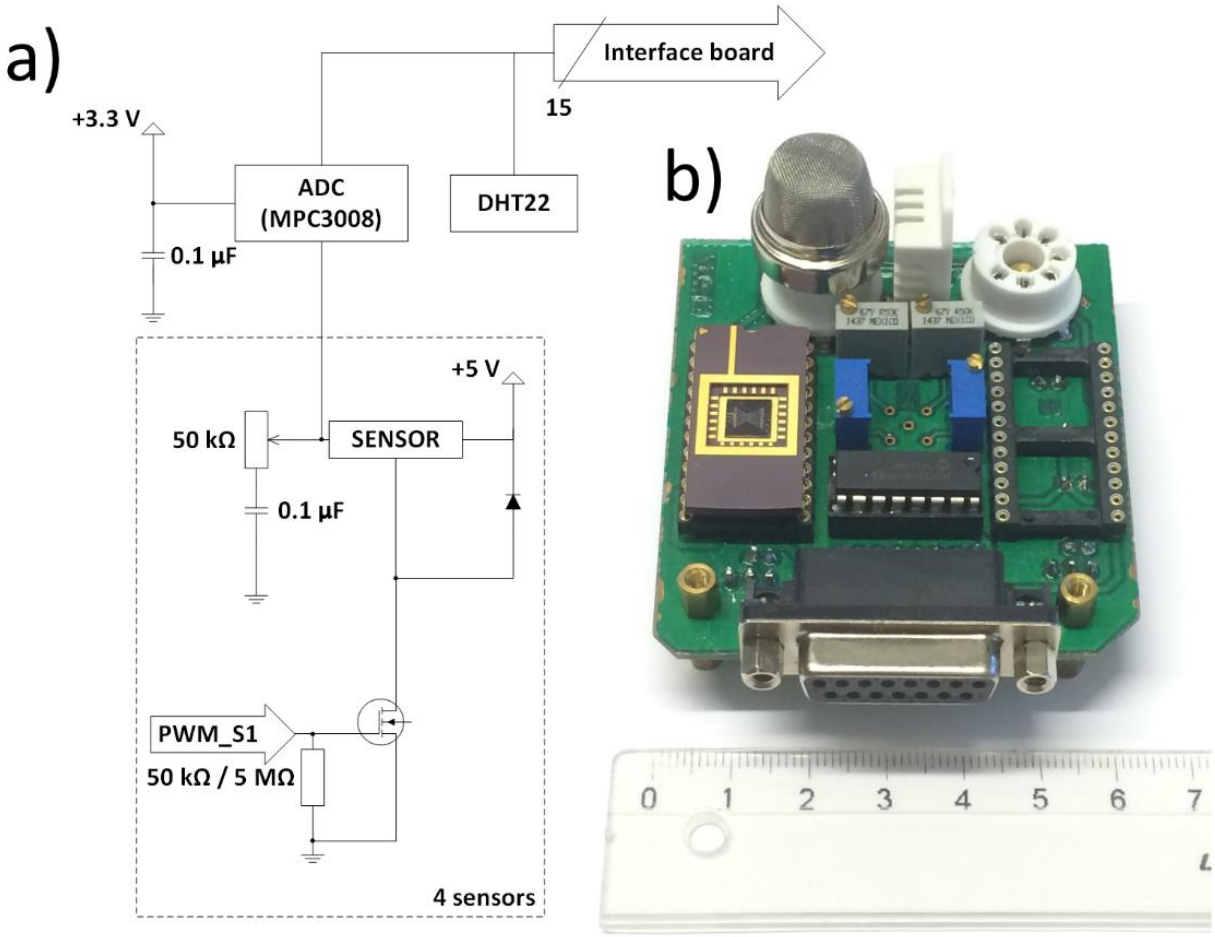

Figure 4 (a) The schematics diagram of the sensor board. The load resistor value depends on the sensor socket type, 50 kΩ for commercial and 5 MΩ for the fabricated sensor. (b) Completed PCB assembly with commercial sensor and experimental sensors occupying upper and lower left slots respectively. The right-side slots are unoccupied.

3. Gas sensors

Nowadays many different metal oxide semiconductors are utilized with different implementations [4,15,16]. In a simplified picture, the principle of the gas sensing with semiconductors is based on redox reactions that take place between target gas and the surface. The interaction results in a change of the concentration of mobile carriers but may also create localization thus influencing the electrical conductivity of the material. The direction of change in conductivity depends on the type of the semiconductor film and the oxidizing or reducing type of gas. In n-type semiconductors oxidizing gas molecules (electron acceptors) decrease the conductivity of the film, whereas reducing gas molecules that act as electron donors increase the conductivity. The effects are reversed in p-type semiconductors [16–18]. These reactions are often enhanced by decorating the semiconductor with metal nanoparticles such as platinum (Pt), palladium (Pd) or gold (Au). These metal particles act as co-catalyst reducing the activation energy in the chemical reactions on the sensing surface [19,20]. In order to evaluate the performance of the CPS, a sensor based on Pt-decorated WO_3 nanoparticles

was made. Tungsten oxide (WO_3) is used extensively in contemporary research and has excellent sensitivity to a wide number of gases [5,21,22].

For the experimental sensor, Pt-decorated WO_3 nanoparticles were prepared following the description in our earlier report [1]. In brief, to produce the sensing material with 1 wt% metal loading, 18 mg of $Pt(C_5H_7O_2)_2$ (platinum acetylacetonate, 99.99%, 523038, Aldrich) was dissolved in 175 mL of acetone and sonicated with 0.875 g of WO_3 nanoparticles (550086, Aldrich) for 2 h. The mixture was then stirred for 4 h at room temperature followed by drying at 150 °C under N_2 flow thus getting WO_3 nanoparticles decorated with the Pt precursor. In a subsequent annealing step at 300 °C for 2 h in air (heating rate of 5 °C/min) the Pt precursor was decomposed to Pt and PtO_x and finally reduced to metallic Pt at 200 °C for 3 h in 15 % H_2/Ar mixture (heating rate of 5 °C/min).

The Pt-decorated WO_3 nanoparticles were characterized via high-resolution transmission electron microscopy imaging (HRTEM, FEI Tecnai G2 20 X-TWIN, 200 kV accelerating voltage) and X-ray diffraction (XRD, Bruker D8 DISCOVERY, Cu Kα radiation). The decomposition of Pt impregnated on the WO_3 nanoparticles resulted in the formation of Pt nanoparticles with typical size of 1-5 nm on the surface, Figure 5(a). The formed Pt nanoparticles show good distribution on WO_3 surface. The obtained XRD pattern for the sensor material is shown in Figure 5(b). The pattern is very similar to that expected for monoclinic WO_3 (JCPDS card #830951) with an additional peak at 38.9° which is associated with the Pt nanoparticles [1]. The low intensity of the Pt peak can be due the small size, low concentration and amorphous structured of the formed Pt nanoparticles.

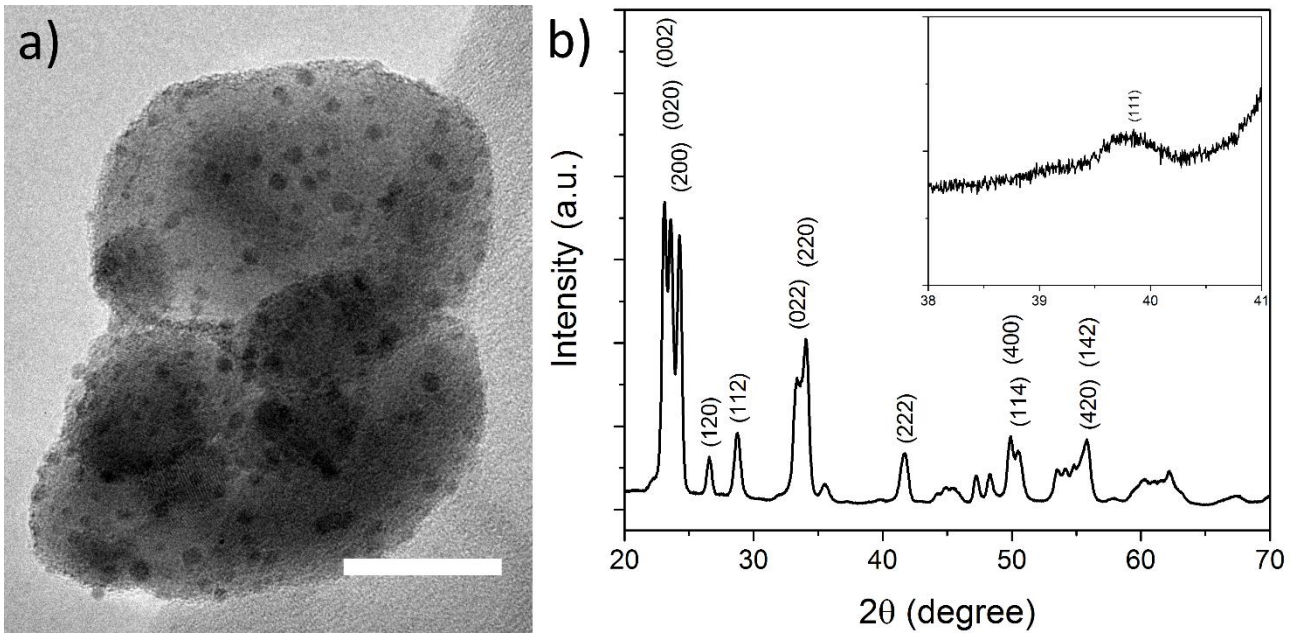

Figure 5 (a) HRTEM image of the Pt-decorated WO_3 nanoparticles. The scale bar shows 20 nm (b) X-ray diffraction pattern of the nanoparticles and the WO_3 peaks. Platinum peak as inset.

For the sensor fabrication, an ink was prepared by sonicating 20 mg of the WO_3-Pt nanoparticles with 20 g of distilled water for 3 hours. The ink was then left to sediment overnight. 2 ml of the supernatant layer of the ink was collected and injected to the inkjet cartridge (Dimatix DMC-11610). The printing

was carried out with a Dimatix DMP-2800 materials printer with ink temperature of 30 °C and platform temperature of 35 °C. The jetting of the nozzle and printing results were optimized by adjusting the firing voltage of the nozzle. A line pattern of 10 vertical points and 20 - 40 layers was deposited on Si/SiO_2 substrates with platinum electrode pattern and a titanium adhesion layer (Figure 6). The subsequent droplets had a 1.8 s delay between each other and there was a 5 s pause between layers. The image shows good coverage of the particles over electrodes. The printed electrode chip was then wire bonded to a dual in-line package (DIP) chip carrier compatible with the sensor board, Figure 6(a).

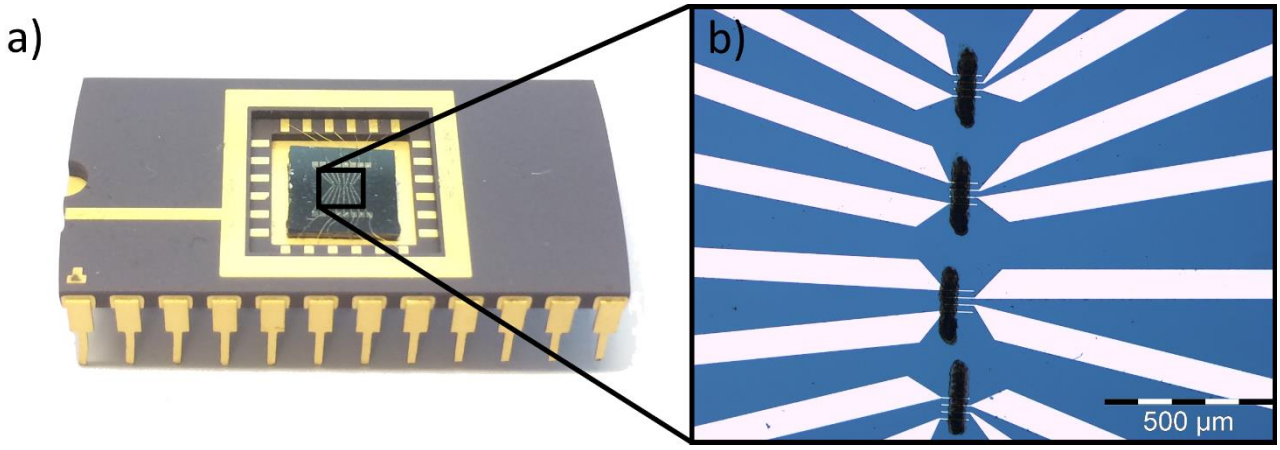

Figure 6 (a) The completed fabricated sensor with a wire bonded sensor chip to a DIP chip carrier. (b) An optical microscope image (Olympus BX51 with Cell^A imaging software, Soft Imaging System GmbH) of the printed sensing layers on the Si microchip.

4. Results and discussion

4.1 System Performance

The systems performance was evaluated by using a customized test chamber with volume of 1500 cm^3 (Figure 7). The chamber could be heated up to maximum 70 °C with a heater block assembly (comprising of a 40 W Kapton® heater foil, finned heat exchanger and an assisting fan for better and faster heat distribution, Figure 7 (c)). In order to validate the system, synthetic air (AGA, 80 % N_2, 20 % O_2) and hydrogen (AGA, 99 % N_2, 1 % H_2) were used as measurement gases. An array of mass flow controllers (MKS Instruments 1179A Mass-Flo®, flow rate of 1-1000 sccm) attached to a PC running a LabVIEW program controlled the concentration pulses during measurements. The sensor board was inserted to the chamber and connected to the measurement platform with a 15-pin serial feedthrough.

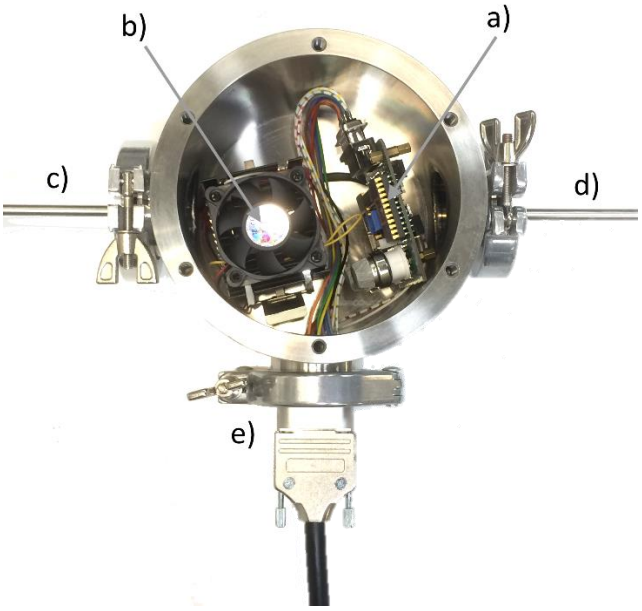

Figure 7: (a) The measurement chamber with the sensor board and (b) heater block assembly. (c) Gas inlet at left, (d) outlet at right and (e) serial cable feedthrough on bottom.

The Raspberry Pi platform was evaluated by utilizing the commercial Taguchi-type sensors in the test chamber at ambient temperature of 22 °C. Several 5 minute long H_2 pulses were applied following 5 min purge cycles with synthetic air. A graphical interface enables the user to evaluate the measurements in real time as shown in Figure 8(a). The raw data was uploaded to the cloud and plotted afterwards using OriginPro (Figure 8(b)). For the Yún platform, gas measurements were performed in two different conditions; (i) in ambient temperature (22 °C), with H_2 concentrations from 50 to 1000 ppm and (ii) with the chamber heated to 70 °C and H_2 concentrations from 100 to 2000 ppm. Total gas flow was a constant 500 sccm for both conditions (Figure 9). Due to the synthetic air used as buffer gas, the chamber humidity was effectively zero during the measurements.

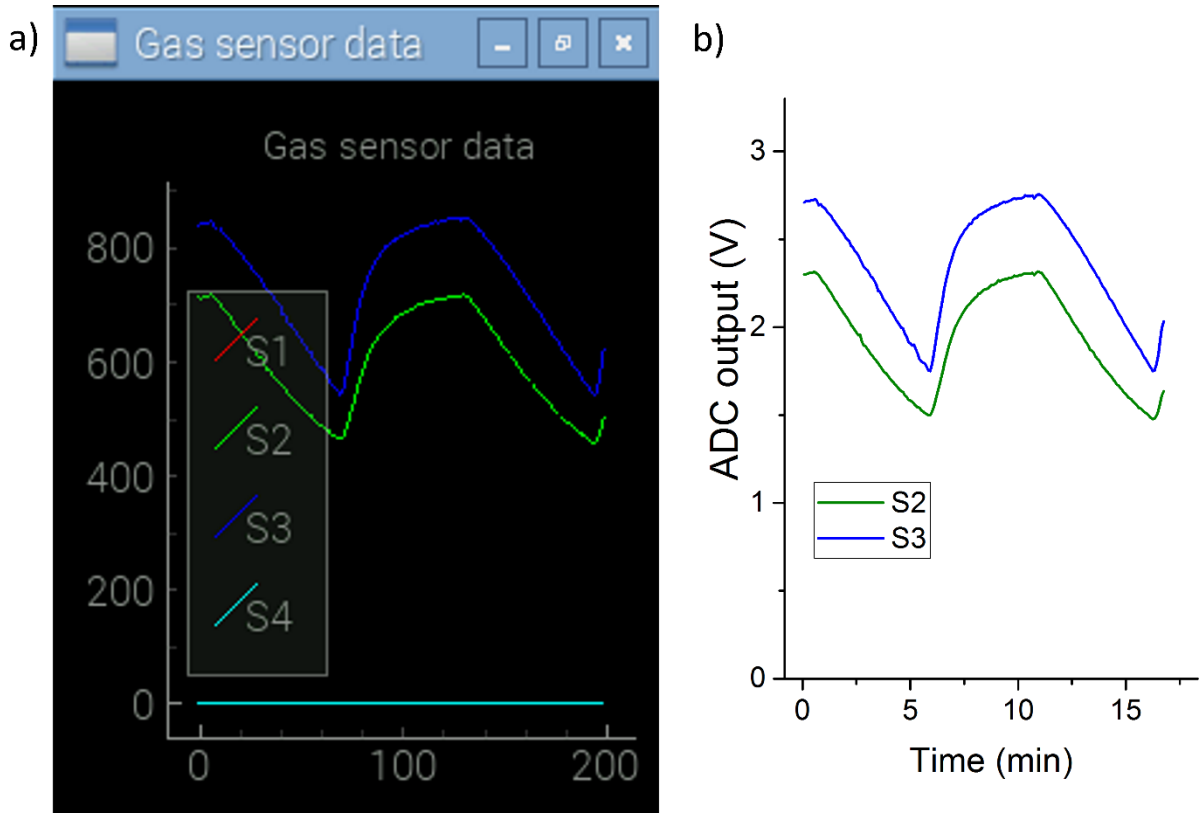

Figure 8 (a) A screenshot from the Raspberry Pi system display during a measurement. (b) The measurement data was later retrieved from the cloud and plotted in OriginPro using actual values. The sampling interval was 5 seconds and ADC output range between 0 and 3.3 V. The DIP sockets (S1 and S4) for fabricated sensors were empty and show no signal. S2 and S3 are the commercial Taguchi sensors MQ-4 and MQ-8, respectively.

The stationary platform also allows for the monitoring in real time through a graphical interface similar to the one developed for the fully wireless system (Figure 8(a)). The raw data collected during the gas measurements was exported as .txt and plotted using OriginPro software (Origin-Lab Corporation, USA) as shown in Figure 9. Our results show that the commercial Taguchi-type sensors respond at all concentrations and temperatures, which clearly demonstrates the operability of both CPS, Figure 9(a). The fabricated Pt-WO_3 nanoparticle sensor showed a response with 1000 and 2000 ppm after heating the chamber to 70 °C, Figure 9(b). This result is in agreement with previous results [1,5]. It is worth mentioning that Taguchi sensors include integrated heater coils, which heat the sensitive metal oxide semiconductor material up to several hundred degree Celsius regardless of the ambient temperature [23]. This explains the low sensitivity of the fabricated Pt-WO_3 nanoparticle sensor in room temperature. In addition, the CPS is limited to external loads with a resistance of not higher than 5 GΩ, with the 5 MΩ load resistance. Therefore the response of the fabricated sensor was "out of range" at lower analyte concentrations. This implies that the platform is suitable for sensor impedances of 1 MΩ or lower. In conclusion, both systems present similar performances achieving the desired operability, however, the fully wireless CPS has the advantage of portability.

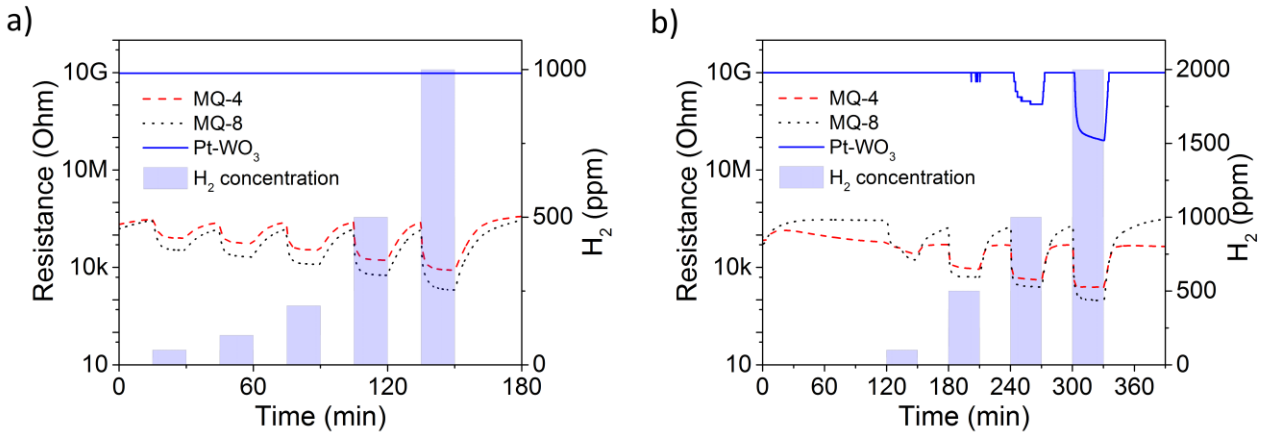

Figure 9. The sensor responses at ambient temperature of 22 °C and H_2 concentrations from 50 to 1000 ppm, (a), and at 70 °C with H_2 concentrations from 100 to 2000 ppm (b). Note: The system had a 5 GΩ measurement limit. Higher impedances gave null signal, which is represented as a flat line in the graphs.

Humidity response of the Pt-WO_3 sensor was appraised by measuring a drop casted sample in a Linkam THMS600 stage at 70 °C using 1000 ppm H_2 pulses. Sensor resistance was measured by Keithley 2636A SYSTEM SourceMeter® sourcing 1 V and measuring current. Humidity was increased by bubbling source gases through deionized water and measured with the DHT22 sensor. The response of the sensor is shown in figure 10. The response to increased humidity is noticeable but it remains significantly minor compared to the gas response.

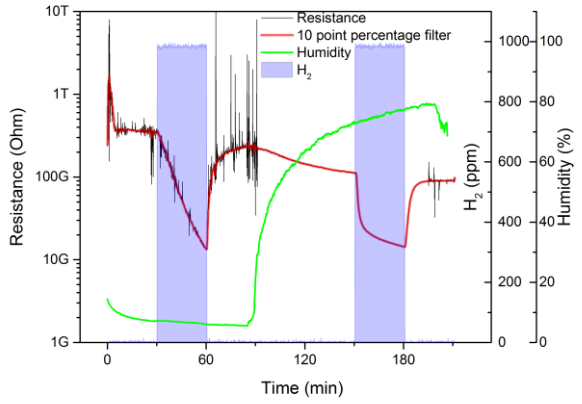

Figure 10. The humidity response of the sensor. The noise from measurement system was reduced by applying a 10 point percentage filter to indicate the actual sensor response. Humidity was introduced to the system at 90 minutes. The humidity is measured as relative humidity (RH). Total gas flow was 200 sccm.

4.2 Future improvements

The electronics design of the presented systems was based on fast prototyping and easily interchangeable components. The layout could be refined further by implementing the design with

mainly surface-mounted components. This would decrease the size and weight of the system considerably. The performance and the amount of used components could also be improved by removing the microcontroller between the ADC and Raspberry Pi. This would simplify the communication interfaces and could allow for omitting the interface board altogether. The heaters would still require a separate PWM controller chip with the low-pass filters. The impedance range of the CPS itself proved to be insufficient with the fabricated sensory type at room temperatures, as the sensing range was limited around 1 nS or 1 GΩ. This could be extended for example with buffering amplifiers.

The envisioned functionality at the proof-of-concept stage such as recording the data and uploading it to cloud was fulfilled. Future operations could be automatized for continuous operation instead of individual experiments. The user interface and general usability could be improved to simplify modifying parameters which are now hard-coded to the program. Measurement performance could be optimized with software improvements such as pulsed measuring and enhancing SNR and resolution by averaging the ADC values [24,25]. The ADC itself could be updated from 10 bits to better resolution, such as 12 or 16 bits. The PWM signal is suitable as such for the Taguchi sensors but it should be filtered with a low-pass filter for the MEMS heater structures to avoid harming the elements at higher voltages. To ensure reliable readings in field conditions, where temperature and humidity vary notably, the tested sensors should be first calibrated at different temperature and humidity values. This data can be then utilized by the system to compensate the readings according to the monitored temperature and humidity.

5. Conclusions

A stationary and a portable CPS were designed, manufactured and validated with both commercial and experimental Taguchi-type sensors. The validation was carried out by measurements at various H_2 concentrations at room and slightly elevated temperatures (22 °C and 70 °C, respectively). Both CPS, stationary and fully wireless, showed good performance and satisfactory operability filling all the specified functionality which they were designed for. The realized sensor board is versatile and suitable for plug-in operation of different types of sensors. The simultaneous measurement data from four different sensors could be used to form a sensor matrix, where the selectivity is improved by comparing the responses of individual sensors. The size of the platform could easily be downscaled by using extensively surface-mounted components. In addition to size and weight factors, the power consumption could be lowered by developing low power sensors and measurement methods.

Acknowledgements

The financial support received from the Hungarian Scientific Research Fund (OTKA) K120115 and GINOP-2.3.2-15-2016-00013, Academy of Finland (projects CNT4Tissue, HyNa and Suplacat), EU-FP7 (HiPPoCaMP) are acknowledged. Aron Dombovari from Microelectronics Research Unit, University of Oulu is acknowledged for the assistance with the humidity test setup.

References

[1] J. Kukkola, M. Mohl, A.-R. Leino, G. Tóth, M.-C. Wu, A. Shchukarev, A. Popov, J.-P.

Mikkola, J. Lauri, M. Riihimäki, J. Lappalainen, H. Jantunen, K. Kordás, Inkjet-printed gas sensors: metal decorated WO_3 nanoparticles and their gas sensing properties, J. Mater. Chem. 22 (2012) 17878. doi:10.1039/c2jm32499g.

[2] J. Kukkola, M. Mohl, A.-R. Leino, J. Mäklin, N. Halonen, A. Shchukarev, Z. Konya, H. Jantunen, K. Kordas, Room temperature hydrogen sensors based on metal decorated WO_3 nanowires, Sensors Actuators B Chem. 186 (2013) 90–95. doi:10.1016/j.snb.2013.05.082.

[3] J.. Solis, S. Saukko, L. Kish, C.. Granqvist, V. Lantto, Semiconductor gas sensors based on nanostructured tungsten oxide, Thin Solid Films. 391 (2001) 255–260. doi:10.1016/S0040-6090(01)00991-9.

[4] H. Meixner, U. Lampe, Metal oxide sensors, Sensors Actuators B Chem. 33 (1996) 198–202. doi:10.1016/0925-4005(96)80098-0.

[5] S.J. Ippolito, S. Kandasamy, K. Kalantar-zadeh, W. Wlodarski, Hydrogen sensing characteristics of WO_3 thin film conductometric sensors activated by Pt and Au catalysts, Sensors Actuators B Chem. 108 (2005) 154–158. doi:10.1016/j.snb.2004.11.092.

[6] G. Heiland, Zum Einfluß von adsorbiertem Sauerstoff auf die elektrische Leitfähigkeit von Zinkoxydkristallen, Zeitschrift Für Phys. (1954). http://link.springer.com/article/10.1007/BF01340692 (accessed November 10, 2015).

[7] A. Bielanski, J. Deren, J. Haber, Electric conductivity and catalytic activity of semiconducting oxide catalysts, Nature. (1957). http://adsabs.harvard.edu/abs/1957Natur.179..668B (accessed November 10, 2015).

[8] T. Siyama, A. Kato, A new detector for gaseous components using semiconductor thin film, Anal. Chem. (1962). https://scholar.google.fi/scholar?q=a+new+detector+for+gaseous+components+using+semiconductive+thin+films&btnG=&hl=en&as_sdt=0%252C5#0 (accessed November 2, 2015).

[9] N. Taguchi, A metal oxide gas sensor, Japanese Pat. (1962). https://scholar.google.fi/scholar?q=related:mJB47i79lpIJ:scholar.google.com/&hl=en&as_sdt=0,5#0 (accessed November 10, 2015).

[10] P. Marwedel, Embedded and cyber-physical systems in a nutshell, DAC. COM Knowl. Cent. Artic. (2010). http://www.researchgate.net/profile/Peter_Marwedel/publication/242741208_Embedded_and_Cyber-Physical_Systems_in_a_Nutshell/links/00b49530cab811296f000000.pdf (accessed November 5, 2015).

[11] A. Usman, H. Mukhtar, Design time considerations for cyber physical systems, in: 2012 IEEE Int. Conf. Green Comput. Commun., IEEE, 2012: pp. 442–445. doi:10.1109/GreenCom.2012.69.

[12] J. Singh, O. Hussain, Cyber-physical systems as an enabler for next generation applications, in: 2012 15th Int. Conf. Network-Based Inf. Syst., IEEE, 2012: pp. 417–422. doi:10.1109/NBiS.2012.106.

[13] R. Baheti, H. Gill, Cyber-physical systems, Impact Control Technol. (2011). http://ieeecss.org/sites/ieeecss.org/files/documents/IoCT-Part3-02CyberphysicalSystems.pdf (accessed October 28, 2015).

[14] PyQtGraph - Scientific graphics and GUI Library for Python, (n.d.). http://pyqtgraph.org/ (accessed February 26, 2016).

[15] C. Wang, L. Yin, L. Zhang, D. Xiang, R. Gao, Metal oxide gas sensors: sensitivity and influencing factors., Sensors (Basel). 10 (2010) 2088–106. doi:10.3390/s100302088.

[16] P. Shankar, J. Rayappan, Gas sensing mechanism of metal oxides: The role of ambient atmosphere, type of semiconductor and gases-A review, ScienceJet. (2015). https://www.researchgate.net/profile/Prabakaran_Sankar/publication/270587471_Gas_sensing_mechanism_of_metal_oxides_The_role_of_ambient_atmosphere_type_of_semiconductor_and_gases_-A_review/links/54afd7080cf253690b0ab176.pdf (accessed February 26, 2016).

[17] S.R. Morrison, Semiconducting-oxide chemical sensors, IEEE Circuits Devices Mag. 7 (1991) 32–35. doi:10.1109/101.75926.

[18] N. Yamazoe, G. Sakai, K. Shimanoe, Oxide semiconductor gas sensors, Catal. Surv. from Asia. 7 (n.d.) 63–75. doi:10.1023/A:1023436725457.

[19] C.-C. Chan, W.-C. Hsu, C.-C. Chang, C.-S. Hsu, Preparation and characterization of gasochromic Pt/WO_3 hydrogen sensor by using the Taguchi design method, Sensors Actuators B Chem. 145 (2010) 691–697. doi:10.1016/j.snb.2010.01.021.

[20] W.-C. Hsu, C.-C. Chan, C.-H. Peng, C.-C. Chang, Hydrogen sensing characteristics of an electrodeposited WO_3 thin film gasochromic sensor activated by Pt catalyst, Thin Solid Films. 516 (2007) 407–411. doi:10.1016/j.tsf.2007.07.055.

[21] M. Takács, C. Dücső, A.E. Pap, Fine-tuning of gas sensitivity by modification of nano-crystalline WO_3 layer morphology, Sensors Actuators B Chem. 221 (2015) 281–289. doi:10.1016/j.snb.2015.06.081.

[22] P.J. Shaver, Activated tungsten oxide gas detectors, Appl. Phys. Lett. 11 (1967) 255. doi:10.1063/1.1755123.

[23] N. Barsan, D. Koziej, U. Weimar, Metal oxide-based gas sensor research: How to?, Sensors Actuators B Chem. 121 (2007) 18–35. doi:10.1016/j.snb.2006.09.047.

[24] S. Kwakye, A. Baeumner, An embedded system for portable electrochemical detection, Sensors Actuators B Chem. 123 (2007) 336–343. doi:10.1016/j.snb.2006.08.032.

[25] J. Candy, G. Temes, Oversampling delta-sigma data converters: theory, design and simulation, (1992). http://www.sidalc.net/cgi-bin/wxis.exe/?IsisScript=UCC.xis&method=post&formato=2&cantidad=1&expresion=mfn=031361 (accessed August 3, 2016).